J Water Environ Nanotechnol 2026, 11(4): 504-521
10.22090/jwent.2026.2077459.2005

RESEARCH PAPER

Magnetically Recoverable TiO_2/Fe_3O_4/ Activated Carbon Photocatalyst with High Reusability for Congo Red Removal

Nurfadini[1], Paulina Taba[1]*, Djabal Nur Basir[1], Nunuk Hariani Soekamto[1], Ahmad Ahyar[1], Yusafir Hala[1], Nur Ahmad[2], Andi Uswatun Hasanah[3] I Wayan Sutapa[4]

[1]Department of Chemistry, Faculty of Mathematics and Natural Science, Hasanuddin University, South Sulawesi, Indonesia
[2]Research Center for Catalysis, National Research and Innovation Agency, Building 452 KST BJ Habibie Serpong, Tangerang Selatan, Banten 15311, Indonesia
[3]Departement of Physics, Faculty of Mathematics and Natural Science, Hasanuddin University, South Sulawesi, Indonesia
[4]Departement of Physics, Faculty of Mathematics and Natural Science, Halu Oleo University, Kampus Hijau Bumi Tridharma, 93232, Kendari, Southeast Sulawesi, Indonesia

*Corresponding Author. Email: paulinataba@unhas.ac.id

Article History:

Received: 2025-11-11

Revised: 2026-01-09

Accepted: 2026-01-27

How to cite this article
Nurfadini, Taba P, Basir D N, Soekamto N H, Ahyar A, Hala Y, Ahmad N, Hasanah A U, Sutapa I W. Magnetically Recoverable TiO_2/Fe_3O_4/ Activated Carbon Photocatalyst with High Reusability for Congo Red Removal. J Water Environ Nanotechnol 2026, 11(4): 504-521, DOI: 10.22090/jwent.2026.2077459.2005

HIGHLIGHTS

- TiO_2/Fe_3O_4/activated carbon composite was synthesized via a simple physical mixing method.
- The composite showed excellent photocatalytic activity for Congo Red (20 mg/L), achieving 96.7% degradation after 180 min of UV irradiation.
- The catalyst retained 72% degradation efficiency after four successive reuse cycles.
- The composite exhibits good stability and easy magnetic separation for recovery.

ABSTRACT

This study employed activated carbon (AC) as a support material to facilitate dye adsorption and Fe_3O_4 as a magnetic component to enable separation and reuse of the photocatalyst. The TiO_2/Fe_3O_4/activated carbon (TiO_2/Fe_3O_4/AC) composite was used for the photocatalytic degradation of Congo Red (CR). Characterization was performed using XRD, FTIR, SEM–EDX, VSM, SAA, TGA–DSC, and UV–DRS. The characterization results revealed that the composite possesses a crystalline structure consisting of anatase TiO_2 and magnetite Fe_3O_4 phases, with TiO_2 and Fe_3O_4 particles homogeneously distributed on the surface and within the pores of the AC. Surface texture analysis confirmed that the composite exhibits a mesoporous structure with surface area and porosity favourable for adsorption and photocatalysis. The composite also demonstrated magnetic properties, facilitating magnetic separation after the photocatalytic process. Photocatalytic efficiency was evaluated by CR degradation, achieving 96.7% efficiency. Moreover, the composite maintained stable performance over four consecutive cycles. These findings demonstrate that the TiO_2/Fe_3O_4/AC exhibits potential as a photocatalyst for the removal of dyes from wastewater.

KEYWORDS: *Congo red (CR); Environmental remediation; Photodegradation; Reusability; TiO_2/Fe_3O_4/AC composite*

©2026 The Author(s). Published by the Iranian Environmental Mutagen Society. This work is licensed under the Creative Commons Attribution 4.0 International License (CC BY 4.0). To view a copy of this license, visit http://creativecommons.org/licenses/by/4.0/.

1. INTRODUCTION

Industrial activities have substantially contributed to the accumulation of organic pollutants in aquatic environments, resulting in a major environmental problem [1]. Among these pollutants, synthetic dyes are a major source of global water contamination. They accounted for about 17–20% of total water pollution [2], [3]. Azo dyes are dominant in industrial applications, comprising nearly 60–70% of all dye usage due to their strong affinity for substrates and vivid color properties [4].

Congo Red (CR), an anionic diazo dye, poses significant health risks as it can degrade into benzidine, a known carcinogen that interacts with DNA [5]. Various methods have been utilised to remove dyes from wastewater, including adsorption, membrane filtration, and advanced oxidation processes (AOP) [6]. Among these, AOP has attracted considerable attention due to its ability to degrade dye molecules into harmless products such as carbon dioxide (CO_2) and water (H_2O) [7]. This method requires the use of photocatalysts. Semiconductor-based photocatalysts, including ZnO, TiO_2, ZnS, and WO_2, have been widely investigated for dye degradation [8], [9], [10], [11]. Among these materials, titanium dioxide (TiO_2) is one of the most widely studied due to its high photocatalytic activity, good chemical stability, non-toxic nature, and relatively low cost [12]. Several studies have also reported that TiO_2 exhibits a relatively high efficiency in degrading dye pollutants [13], [14], [15]. However, TiO_2 photocatalysts have inherent drawbacks, particularly their low specific surface area and limited active sites, which reduce adsorption capacity and photocatalytic performance [16]. To address these limitations, TiO_2 is often combined with high-surface-area porous materials such as zeolites, clays, AC, or chitosan. These composite materials significantly enhance dye adsorption and overall photocatalytic efficiency [17], [18], [19], [20].

Activated carbon is widely used as a support material for catalysts because it offers a large surface area, abundant surface functional groups, and high porosity [21]. In photocatalysis, pollutants are adsorbed onto the catalyst's surface, where they are degraded into harmless substances, such as CO_2 and H_2O, by reactive oxygen species, including hydroxyl radicals and superoxide anions [1]. The integration of AC into TiO_2-based photocatalysts facilitates the separation of electron-hole pairs, reduces the rate of recombination, prolongs electron lifetime, and enhances overall photocatalytic performance [21]. Nevertheless, a significant drawback of TiO_2 photocatalysts is the difficulty in recovering the material after photocatalytic reactions, which impacts their reusability [22]. Incomplete retrieval could lead to residual catalyst particles leaching into aquatic ecosystems, posing potential ecological risks to both organisms and humans [23]. An effective approach to address this challenge is the combination of TiO_2 with magnetic particles, which facilitates facile separation using a magnetic field after photocatalysis [24]. The incorporation of magnetic materials, such as Fe_3O_4, not only aids in catalyst recovery and reuse but also enhances energy efficiency and simplifies operational procedures [25].

Several studies have demonstrated that incorporating TiO_2 with magnetic Fe_3O_4 enables efficient photocatalyst separation after the reaction while maintaining high photocatalytic activity. For instance, magnetic AC functionalized with TiO_2 showed excellent degradation performance toward indigosol green dye and effectively reduced Cr(VI) in aqueous solution [11]. Similarly, Fe_3O_4@TiO_2@zeolite nanocomposites exhibited high adsorption efficiency for the antibiotic levofloxacin and demonstrated good reusability over multiple cycles, attributed to the porous zeolite structure and magnetic properties of Fe_3O_4 [26]. Fe_3O_4@TiO_2-based magnetic photocatalysts have also been successfully employed for degrading enrofloxacin and other organic compounds under both UV and visible light irradiation [24]. Another study explored visible-light-active $Fe_3O_4/SiO_2/TiO_2$ composites for 4-nitrophenol degradation, showing good stability through multiple reuse cycles [27]. Despite these advances, studies on TiO_2/Fe_3O_4 composites supported on biomass-derived AC have rarely focused on CR degradation, particularly in terms of systematic photocatalyst reusability evaluation. Therefore, this study offers novelty through the utilisation of corn cob-derived AC as an adsorptive support, the application of TiO_2/Fe_3O_4/AC composites for CR degradation, and a systematic evaluation of photocatalyst stability and reusability, thereby contributing to the development of practical magnetic photocatalysts for dye wastewater treatment.

In this work, TiO_2/Fe_3O_4/AC composites were prepared using corn cob-based AC via a simple, cost-effective, and energy-efficient physical mixing method. The AC functioned as an adsorptive support to enhance dye uptake, while Fe_3O_2 imparted magnetic properties that enabled efficient separation and recovery of the photocatalyst after the reaction. Furthermore, the structural characteristics, morphology, magnetic behaviour, and photocatalytic performance of the composites were systematically evaluated through CR degradation experiments, with emphasis on both efficiency and reusability.

2. METHODOLOGY

2.1 Materials

The photocatalysts materials used in this study are corn cobs, titanium tetra isopropoxide (TTIP) $Ti(OCH(CH_3)_2)_4$ (Sigma-Aldrich), isopropyl alcohol (Merck), ethanol (Merck), sodium hydroxide (NaOH) (Merck), iron(III) chloride ($FeCl_3{\cdot}6H_2O$) (Merck), iron(II) sulfate ($FeSO_4{\cdot}7H_2O$) (Merck), ammonium (NH_3) (Merck), citric acid (Merck), hydrochloric acid (HCl) (Merck), Congo Red (CR) $C_{32}H_{22}N_6Na_2O_6S_2$ (Merck).

2.2 Preparation of activated carbon

The synthesis was carried out based on the method of Lala et al. [28], with some modifications. Corn cobs were initially cleaned and subsequently dried under direct sunlight for three days. The dried materials were then placed in an oven and heated at 100°C for 24 hours. Following this thermal treatment, the samples were carbonized in a furnace at 400°C for 2 hours. The resulting charcoal was ground and sieved using a 200-mesh sieve. Chemical activation was performed by soaking the charcoal in 1 mol/L NaOH solution for 24 hours at room temperature, followed by neutralization. Finally, the product was dried in an oven at 100°C for 6 hours.

2.3 Synthesis of Fe_3O_4

The synthesis was conducted following the method described by Ahmad et al. [29]with slight modifications. A solution was prepared by dissolving $FeCl_3$ and $FeSO_4{\cdot}7H_2O$ in distilled water at a Fe^{3+}: Fe^{2+} molar ratio of 2:1. The solution, with a total volume of 20 mL, was stirred using a magnetic stirrer until complete dissolution was achieved. Ammonia (NH_3) was carefully added dropwise under continuous stirring until the pH reached 10, resulting in precipitate formation. The mixture was then transferred to an autoclave and heated at 160°C for 2.5 hours. The resulting precipitate was washed three times with distilled water and subsequently dried in an oven at 80°C for 1 hour.

2.4 Synthesis of TiO_2

The synthesis was carried out based on the method of Ramalingam [30], with some modifications. A 5 mL aliquot of TTIP precursor was mixed with 25 mL of isopropanol under continuous stirring to ensure thorough blending. Subsequently, 0.1 mol/L acetic acid was added dropwise under continuous stirring until a precipitate formed. The mixture was then placed

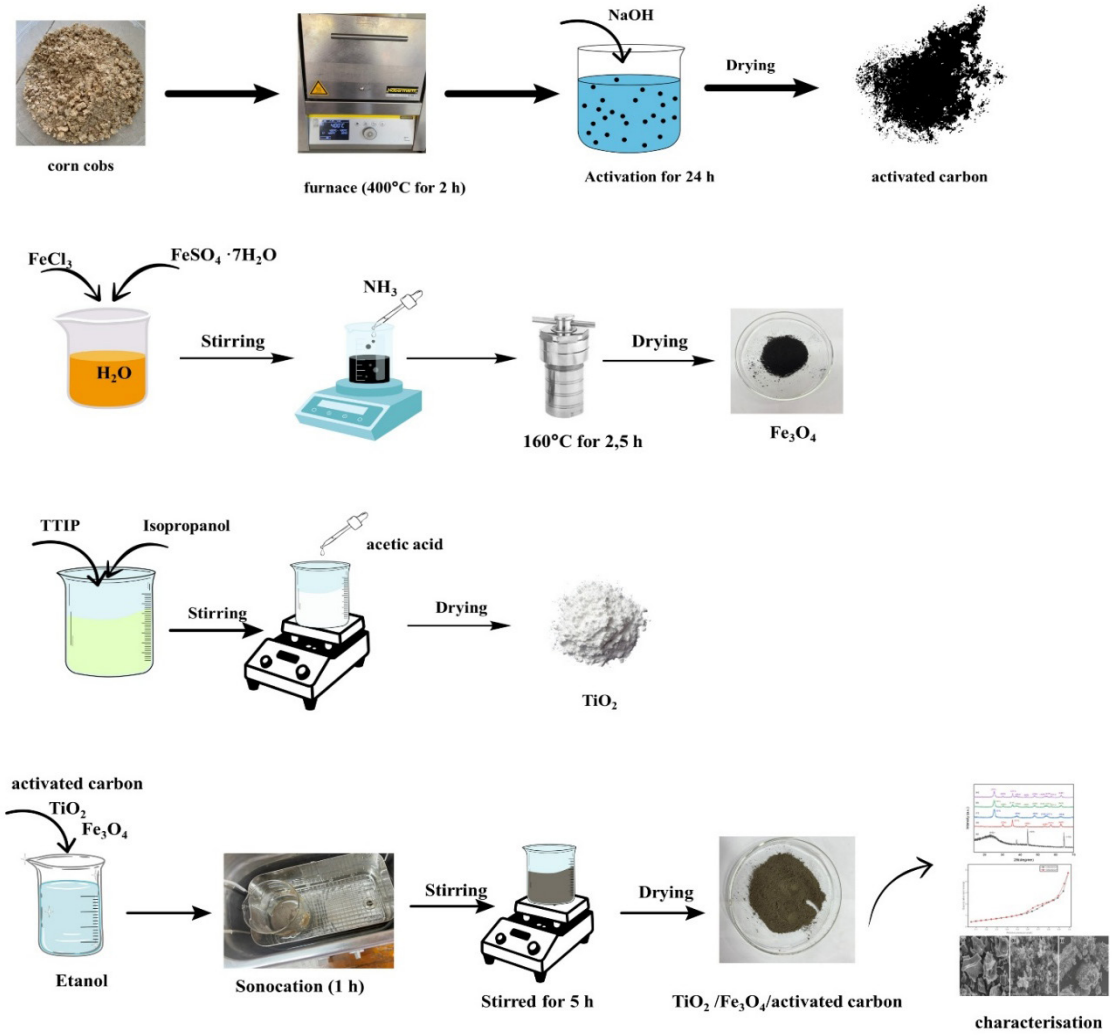


Fig. 1. Schematic of the experimental setup used for synthesizing TiO_2/Fe_3O_4/AC.

J Water Environ Nanotechnol, 2026, 11(4): 504-521
10.22090/jwent.2026.2077459.2005

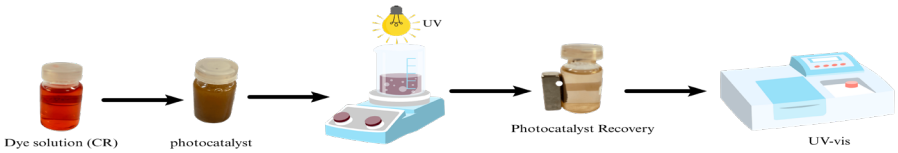


Fig. 2. Schematic of the experimental setup for the photocatalytic degradation process using TiO_2/Fe_3O_4/AC

in an oven and heated at 80°C for 48 hours. Once dried, the powder was transferred to a porcelain crucible and calcined in a furnace at 400°C for 3 hours.

2.5 Synthesis of TiO_2/Fe_3O_4 and TiO_2/Fe_3O_4/AC

The composite synthesis was performed following the method described by Utami et al. [11], with slight modifications. Both TiO_2/Fe_3O_4 and TiO_2/Fe_3O_4/AC composites were prepared using a simple physical mixing method. The TiO_2/Fe_3O_4 composite was synthesized by mixing 1.67 g of Fe_3O_4 and 3.33 g of TiO_2 in 30 mL of isopropanol. The mixture was subjected to ultrasonication for 1 hour to obtain a homogeneous suspension, followed by vigorous stirring for 5 hours. The suspension was then filtered and dried in an oven at 80°C for 4 hours. Similarly, the TiO_2/Fe_3O_4/AC composite was prepared by combining 1.11 g of Fe_3O_4, 1.67 g of AC, and 2.22 g of TiO_2 in 30 mL of isopropanol. The mixture underwent ultrasonication for 1 hour to ensure uniform dispersion, followed by stirring for 5 hours, filtration, and drying at 80°C in an oven for 4 hours. **Fig. 1** illustrates the schematic diagram for the synthesis of TiO_2/Fe_3O_4/AC composite.

2.6 Characterization

The materials were characterized using X-ray diffraction (XRD) on a Shimadzu Maxima-X 7000 diffractometer with CuKα radiation (λ = 1.54 Å). Measurements were performed over a 2θ range of 10°–70° at 40 kV and 30 mA. Fourier Transform Infrared (FTIR) spectroscopy was conducted using a Shimadzu IR Prestige-21 spectrometer over a wavenumber range of 300–4000 cm^{-1}. The morphology of the TiO_2/Fe_3O_4/AC catalyst was examined using Scanning Electron Microscopy (SEM, SU3500) at magnifications ranging from 1,000× to 15,000×, coupled with Energy Dispersive X-ray Spectroscopy (EDX) for elemental analysis. The magnetic properties of the composites were measured using a Vibrating Sample Magnetometer (VSM) at room temperature over a magnetic field range of -1 to 1 T. Ultraviolet-visible diffuse reflectance spectroscopy (UV-DRS, UV3600) was employed to investigate the optical absorption spectrum across wavelengths of 200–800 nm. The specific surface area was determined using a Surface Area Analyzer (SAA). Before measurement, the samples were degassed at 300°C for 4 hours using an Almita Micro-200 Surface Area Analyzer. The thermal properties of the materials were assessed using Thermogravimetric Analysis (TGA) and Differential Scanning Calorimetry (DSC) with a Linseis STA PT1600 instrument. The samples were heated at a rate of 20°C/min up to 1000°C under a nitrogen atmosphere.

2.7 Photocatalytic activity

The photocatalytic procedure was carried out with a 250-watt mercury lamp positioned 25 cm above the reaction solution. In each experiment, 0.1 g of either the photocatalyst composite, TiO_2/Fe_3O_4 or TiO_2/Fe_3O_4/AC, was added to 25 mL of a CR solution with a concentration of 20 mg/L in separate beakers. The solution was exposed to lamp irradiation while being continuously stirred for a duration of 3 hours. After irradiation, the composite was separated using an external magnet. The absorbance of the solution was measured at the maximum absorbance wavelength of CR (499 nm) using a UV–Vis spectrophotometer to calculate the degradation efficiency according to the following equation (1)

$$\%\ \text{degradation} = \frac{C_0 - C_t}{C_0}\ x100\% \qquad (1)$$

C_0 represents the initial concentration of CR dye (mg/L), while Ct refers to the concentration after treatment. **Fig. 2.** Illustration of the photocatalytic degradation process using TiO_2/Fe_3O_4/AC.

2.8 Photocatalyst reusability

To assess the reusability of the photocatalyst, the material was retrieved using a commercial magnet, cleansed with distilled water, oven-dried at 70°C, weighed, and subsequently reintroduced to the CR solution [31].

3. RESULTS AND DISCUSSION

3.1 X-Ray Diffraction (XRD)

The structural characteristics of AC, TiO_2, Fe_3O_4, and the composites were examined using XRD, as depicted in **Fig. 3**. The XRD spectrum of AC exhibits a broad diffraction band in the 2θ range of 10°–30°, indicating an amorphous nature due to the disordered carbon structure. However, the presence of peaks at 24.11°, 44.27°, and 64.61°, corresponding to the (002), (101), and (110) planes, respectively, suggests that the AC still retains a small fraction of micro-graphitic structures. Thus, the AC can be characterized as semi-amorphous with nanometer-sized graphitic domains [32]. **Fig. 3(b)** presents the XRD spectrum of Fe_3O_4, which displays six distinct peaks at 2θ angles of 30.24°

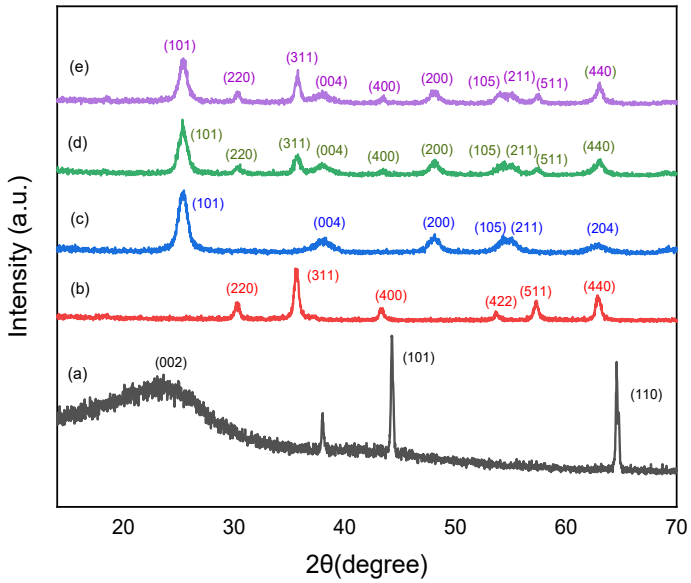


Fig. 3. XRD patterns of **(a)** activated carbon, **(b)** Fe_3O_4, **(c)** TiO_2, **(d)** TiO_2/Fe_3O_4, and **(e)** TiO_2/Fe_3O_4/AC

(220), 35.63° (311), 43.28° (400), 53.70° (422), 57.28° (511), and 62.88° (440). These diffraction patterns are consistent with the cubic crystal structure of magnetite, as referenced in JCPDS card No. 19-0629 [31].

Fig. 3(c) shows the XRD spectrum of TiO_2, while **Figs. 3(d-e)** display the diffraction peaks of TiO_2/Fe_3O_4 and TiO_2/Fe_3O_4/AC composites at 2θ values of 25.2° (101), 37.97° (004), 48.11° (200), 54.07° (105), 55.00° (211), and 63.02° (204), indicating that TiO_2 exists in the anatase phase (JCPDS No. 21-1272) [33]. Additional peaks at 30.33° (220), 35.73° (311), and 57.42° (511) confirm the presence of magnetic Fe_3O_4 particles (JCPDS No. 19-0629) [31], [33]. These results suggest that the anatase phase is the dominant crystalline phase in the composites, while AC is not detected in the XRD spectra due to its amorphous nature. The crystallite size of the materials was determined using the Scherrer equation (Equation 2) with K = 0.9 and λ = 0.15406 nm [34]. The average crystallite size of the TiO_2/Fe_3O_4/AC composite is 8.25 nm, while that of TiO_2/Fe_3O_4 is 10.65 nm. These results indicate that the synthesized materials exhibit nanoscale morphology.

$$D = \frac{K}{\beta \, Cos\, \theta} \quad (2)$$

where

D = average crystallite size (nm)

K = Scherrer constant (0.9)

β = full width at half maximum (FWHM) of the diffraction peak (radians)

θ = Bragg diffraction angle (degrees)

The size of the crystal particles plays a crucial role in determining photocatalytic efficiency, as it influences both surface area and adsorption capacity. Smaller crystals provide a larger surface area, enhancing adsorption and improving the material's ability to degrade dyes. In addition, reduced crystal sizes decrease the recombination rate of electron-hole pairs (e^--h^+), further enhancing photocatalytic performance [35].

3.2 Fourier Transform Infrared (FTIR)

Fig. 4(a) shows the FTIR spectrum of AC, displaying several distinct absorption bands. The broad peak at 3417 cm^{-1} is attributed to O–H stretching vibrations, indicating the presence of hydroxyl groups and suggesting hydrogen bonding likely due to adsorbed water molecules on the AC surface. The band at 2922 cm^{-1} corresponds to C–H stretching vibrations from aliphatic hydrocarbons. The band at 1702 cm^{-1} is assigned to C=O stretching vibrations, attributed to carbonyl, carboxylate, and lactone groups. The band at 1606 cm^{-1} relates to C=C vibrations, reflecting the aromatic structure in AC. The band at 1222 cm^{-1} indicates C–O stretching vibrations found in esters, phenolic compounds, carboxylic acids, and alcohols. The bands at 524 cm^{-1} and 441 cm^{-1} are associated with C–C stretching vibrations [36]. **Fig. 4(b)** reveals a prominent absorption band at 590 cm^{-1}, attributed to Fe–O stretching in Fe_3O_4 [37]. **Fig. 4(c)** presents a peak at 582 cm^{-1}, assigned to Ti–O stretching. The peaks at 3419 cm^{-1} and 1635 cm^{-1} correspond to the bending and stretching of –OH groups, respectively, indicating

J Water Environ Nanotechnol, 2026, 11(4): 504-521
10.22090/jwent.2026.2077459.2005

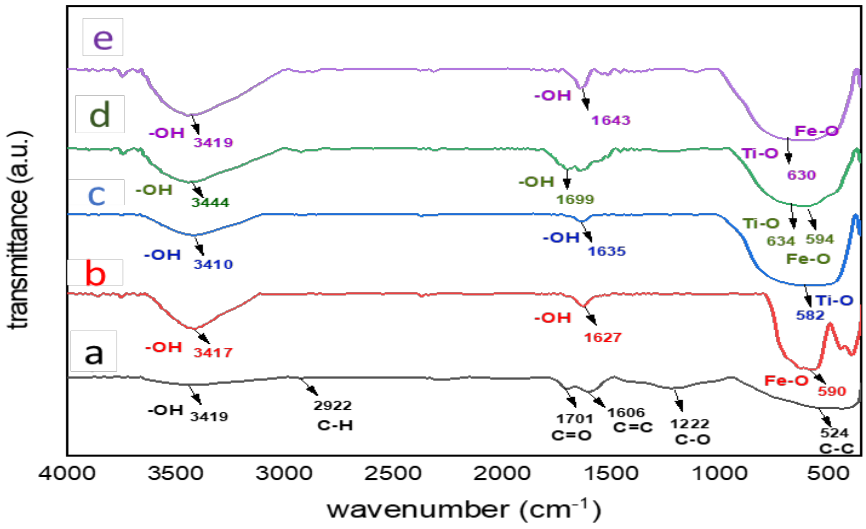


Fig. 4. FTIR of **(a)** activated carbon, **(b)** Fe_3O_4, **(c)** TiO_2, **(d)** TiO_2/Fe_3O_4, **(e)** TiO_2/Fe_3O_4/AC

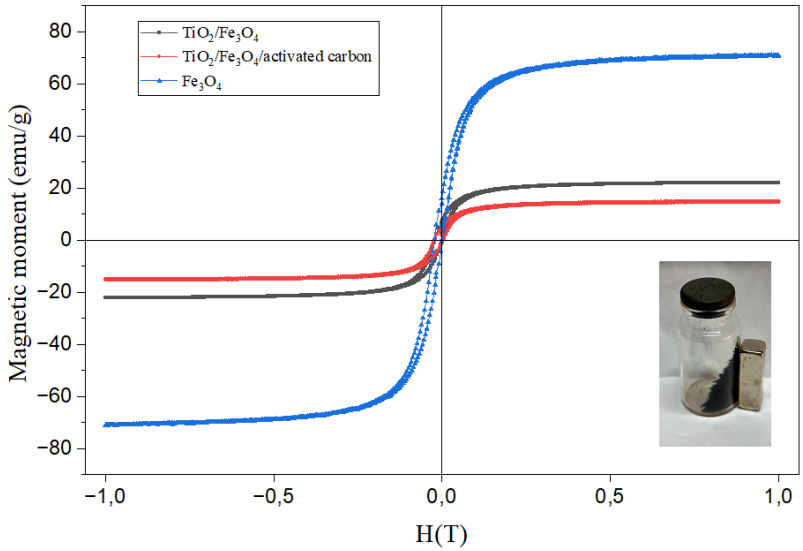


Fig. 5. Magnetic properties of Fe_3O_4, TiO_2/Fe_3O_4, and TiO_2/Fe_3O_4/AC in vibrating sample magnetometer (VSM) testing

the presence of adsorbed water molecules in the composite [38]. The FTIR spectra of both composites feature broad bands between 500 and 800 cm^{-1}, representing Ti–O–Ti stretching vibrations. The breadth of these bands likely results from overlapping Ti–O and Fe–O peaks, confirming the successful integration of the composite components [33].

3.3 Vibrating Sample Magnetometry (VSM)

The magnetic behavior of the synthesized photocatalysts was evaluated using VSM at room temperature under an applied magnetic field ranging from −1 to 1 T. The magnetic properties of the materials are presented in **Fig. 5**, showing that the saturation magnetization values for Fe_3O_4, TiO_2/Fe_3O_4, and TiO_2/Fe_3O_4/AC are 70.71 emu/g, 22.13 emu/g, and 14.78 emu/g, respectively. The decrease in saturation magnetization is attributed to the presence of non-magnetic AC and TiO_2 layers on the Fe_3O_4 surface, as indicated by the hysteresis curves. Both composites retain superparamagnetic properties, with negligible coercivity values close to zero, suggesting their potential applicability in applications requiring magnetic separation [39].

3.4 Ultraviolet-Visible Diffuse Reflectance Spectroscopy (UV-DRS)

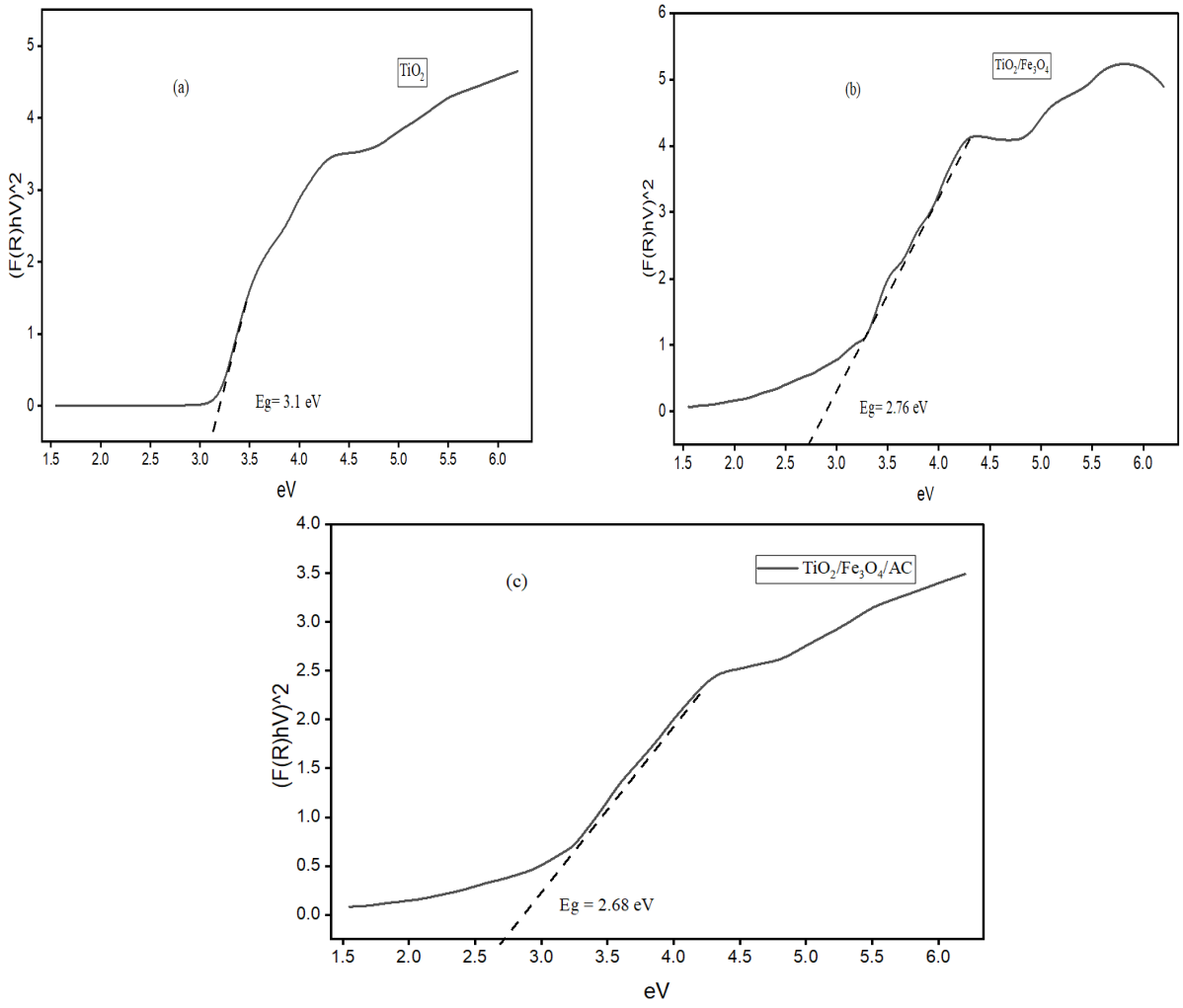


Fig. 6. UV-DRS of **(a)** TiO2, **(b)** TiO_2/Fe_3O_4, dan **(c)** TiO_2/Fe_3O_4/AC

UV-DRS analysis of TiO_2, TiO_2/Fe_3O_4, and TiO_2/Fe_3O_4/AC was conducted in the wavelength range of 200–800 nm to evaluate their optical properties. The band gap energy (Eg) was determined using the Kubelka–Munk method to elucidate the optical characteristics of each material. As illustrated in **Fig. 6**, the Eg values for TiO_2, TiO_2/Fe_3O_4, and TiO_2/Fe_3O_4/AC are 3.1 eV, 2.76 eV, and 2.68 eV, respectively. The lower band gap energy in the composites indicates enhanced visible light absorption capability, thereby improving their photocatalytic effectiveness compared to pristine TiO_2. Therefore, the incorporation of Fe_3O_4 and AC into TiO_2 increases its light absorption capacity, enhancing its performance in photocatalytic applications.

3.5 Surface Area Analyzer (SAA)

The surface textural properties of the AC and TiO_2/Fe_3O_4/AC composite, including specific surface area, pore volume, and pore size distribution, were analyzed using SAA. The isotherm curves of AC and TiO_2/Fe_3O_4/AC exhibit a typical type IV pattern, indicating the presence of mesoporous structures (**Figs. 7a and 7c**). AC exhibits a high specific surface area of 211.6 m^2/g with a relatively small pore volume (0.15 cm^3/g) and an average pore diameter of 2.8 nm, indicating the dominance of mesoporous structures. In contrast, the TiO_2/Fe_3O_4/AC composite shows a lower specific surface area of 115 m^2/g but with an increased pore volume of 0.30 cm^3/g and an enlarged average pore diameter of approximately 12 nm, suggesting a more pronounced mesoporous contribution. These differences indicate that although the surface area decreases due to partial pore blockage by metal oxides, the composite retains its effectiveness in adsorbing larger molecules, facilitating reactant diffusion, and enhancing photocatalytic activity.

J Water Environ Nanotechnol, 2026, 11(4): 504-521
10.22090/jwent.2026.2077459.2005

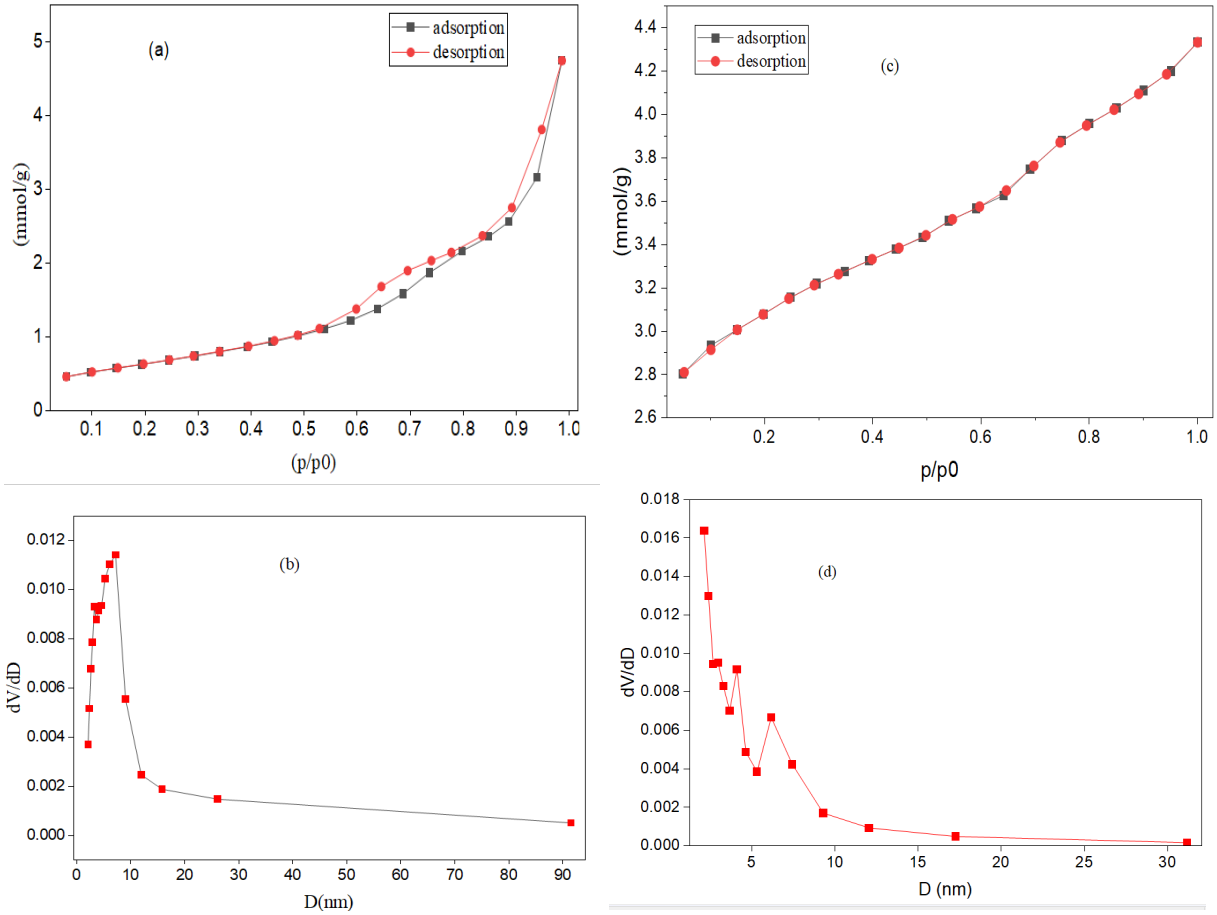


Fig. 7. Adsorption-desorption isotherms of N_2 from Activated Carbon **(a)** and TiO_2/Fe_3O_4/ AC **(c)**. Pore size distribution of Activated Carbon **(b)** and TiO_2/Fe_3O_4/AC **(d)**.

3.6 Thermogravimetric Analysis (TGA) and Differential Scanning Calorimetry (DSC)

TGA-DSC analysis was performed to assess the thermal stability of the synthesized composites. The measurements were carried out under a nitrogen (N_2) atmosphere with a constant heating rate of 10°C min^{-1} over the temperature range of 30–1000°C. As shown in **Fig. 8a**, TiO_2 experienced a slight weight loss of approximately 2.89% up to 1000°C due to the evaporation of adsorbed water and decomposition of residual solvent, indicating its high thermal stability [40]. The DSC curve shows an endothermic peak at 51.91°C, an exothermic peak at 688°C corresponding to anatase crystallization, and another endothermic peak at 714°C related to the anatase-to-rutile phase transformation, which typically occurs between 600–800°C and affects TiO_2's photocatalytic performance [41]. As shown in **Fig. 8b**, Fe_3O_4 exhibits minor weight losses between 76–400°C due to adsorbed water, residual solvent, or minor by-products formed during synthesis, with stabilization observed above 500°C. The DSC curve exhibited an endothermic peak at 116°C, indicative of initial dehydration, and another peak at 265°C, likely associated with the removal of residual solvent or minor by- products from the synthesis process. A strong exothermic peak at 560°C indicates the oxidation of Fe_3O_4 to hematite (α-Fe_2O_3), suggesting enhanced crystallinity and thermal stability due to the formation of a more thermodynamically stable crystalline phase [42], [43]. In **Fig. 8c**, the TiO_2/Fe_3O_4/AC composite exhibits two stages of weight loss—3.64% at 60–200°C and 11.67% at 450–860°C—attributed to the evaporation of water and the degradation of organic groups, primarily from the AC. The absence of exothermic peaks indicates that no new crystallization occurred, suggesting the composite maintains thermal stability even at elevated temperatures.

3.7 Scanning Electron Microscope (SEM)

Fig. 9 illustrates the surface morphology of AC, TiO_2, Fe_3O_4, TiO_2/Fe_3O_4, and TiO_2/Fe_3O_4/AC composites, highlighting the

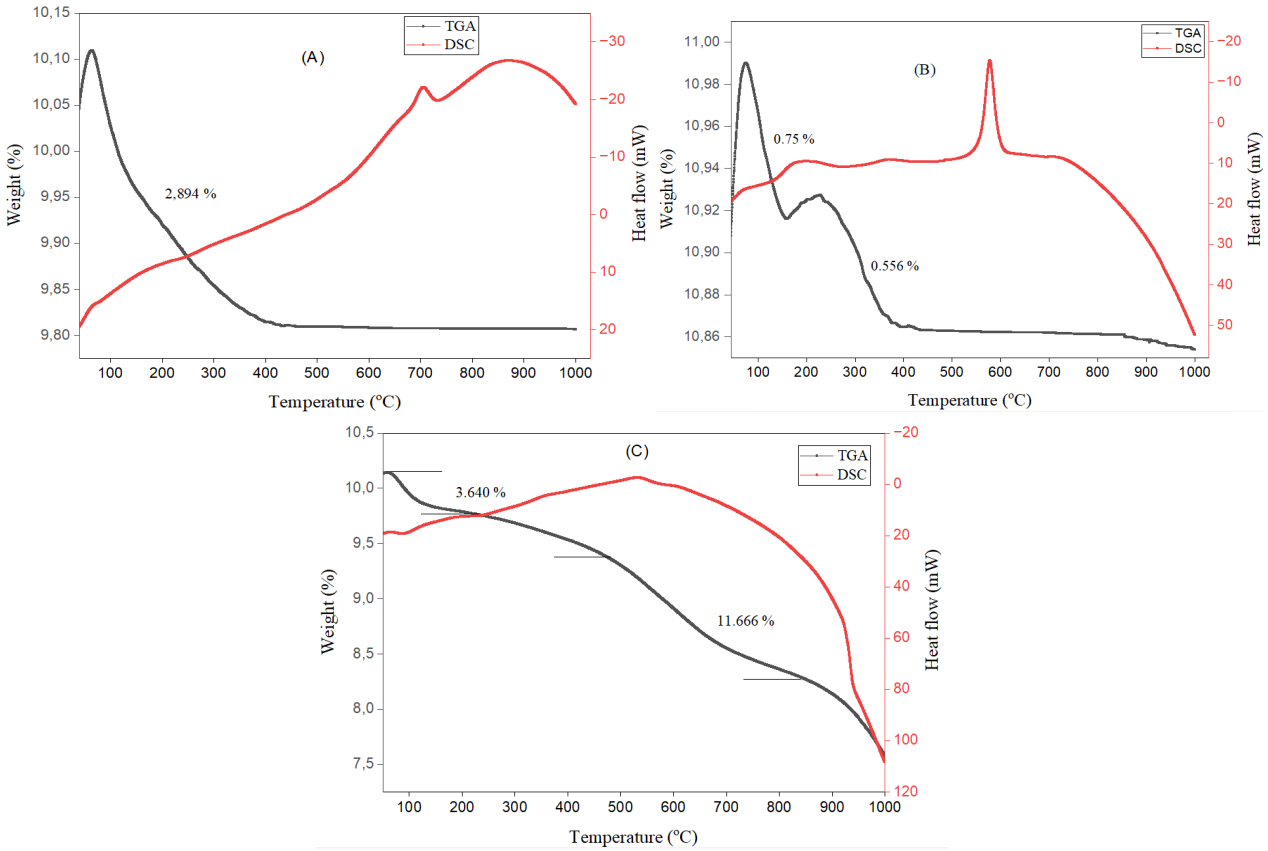


Fig. 8. DSC and TGA analyses of TiO_2 **(a)**, Fe_3O_4 **(b)**, and TiO_2/Fe_3O_4/AC composite **(c)**.

structural alterations that occurred during synthesis. In **Figs. 9a** and **9e**, AC particles display a porous structure that undergoes physical transformation upon the incorporation of TiO_2 and Fe_3O_4. The integration of these components resulted in the formation of new particles that attach to the AC framework, particularly filling the previously vacant spaces and pores. TiO_2 and Fe_3O_4 particles are distributed on the pores and surface of the AC, indicating an increase in active sites on the catalyst's surface. This allows the dye molecules to penetrate the AC's pores and interact with the TiO_2 particles, a critical prerequisite for the catalytic reaction [32]. With TiO_2 particles present on the catalyst surface, the photocatalytic reaction becomes more efficient, as these particles act as active centers for light absorption and electron-hole pair generation [39].

The SEM image of TiO_2 (**Fig. 9b**) reveals a morphology consisting of fine, small-sized granules that tend to form slight agglomerations. In contrast, the SEM image of Fe_3O_4 (**Fig. 9c**) displays irregular particle aggregates with relatively larger dimensions, indicating strong agglomeration typically attributed to magnetic interactions among Fe_3O_4 particles. The EDX spectrum for activated carbon and TiO_2/Fe_3O_4/AC provides insight into the elemental composition of the synthesized samples. **Fig. 9f** confirms that Ti, Fe, C, and O are present as indicated in the table. EDX analysis determined the mass percentage of these elements in the synthesized sample, validating their integral role in the photocatalyst structure. Furthermore, SEM-EDS elemental mapping of the TiO_2/Fe_3O_4/AC composite (**Figs. 9g–k**) demonstrates that Ti and Fe elements are uniformly distributed and overlapped with the carbon matrix across the observed surface. This confirms that TiO_2 and Fe_3O_4 particles were successfully deposited onto the AC surface, thereby partially blocking its pores.

3.8 The Photodegradation Activity of the Material Studied

At the initial stage (adsorption under dark conditions for 30 minutes), the concentration of CR decreased due to adsorption between CR molecules and the photocatalyst surface. The adsorption efficiencies of each photocatalyst were 18.9% for TiO_2/Fe_3O_4 and 51.5% for TiO_2/Fe_3O_4/AC, as shown in **Fig. 10**. For comparison, pure AC showed an adsorption efficiency of 75% under the same conditions, indicating its strong ability to attract CR molecules to its surface. After the adsorption stage, UV irradiation for 180 minutes initiated the actual photocatalytic process.

The control experiment, conducted without a photocatalyst,

J Water Environ Nanotechnol, 2026, 11(4): 504-521
10.22090/jwent.2026.2077459.2005

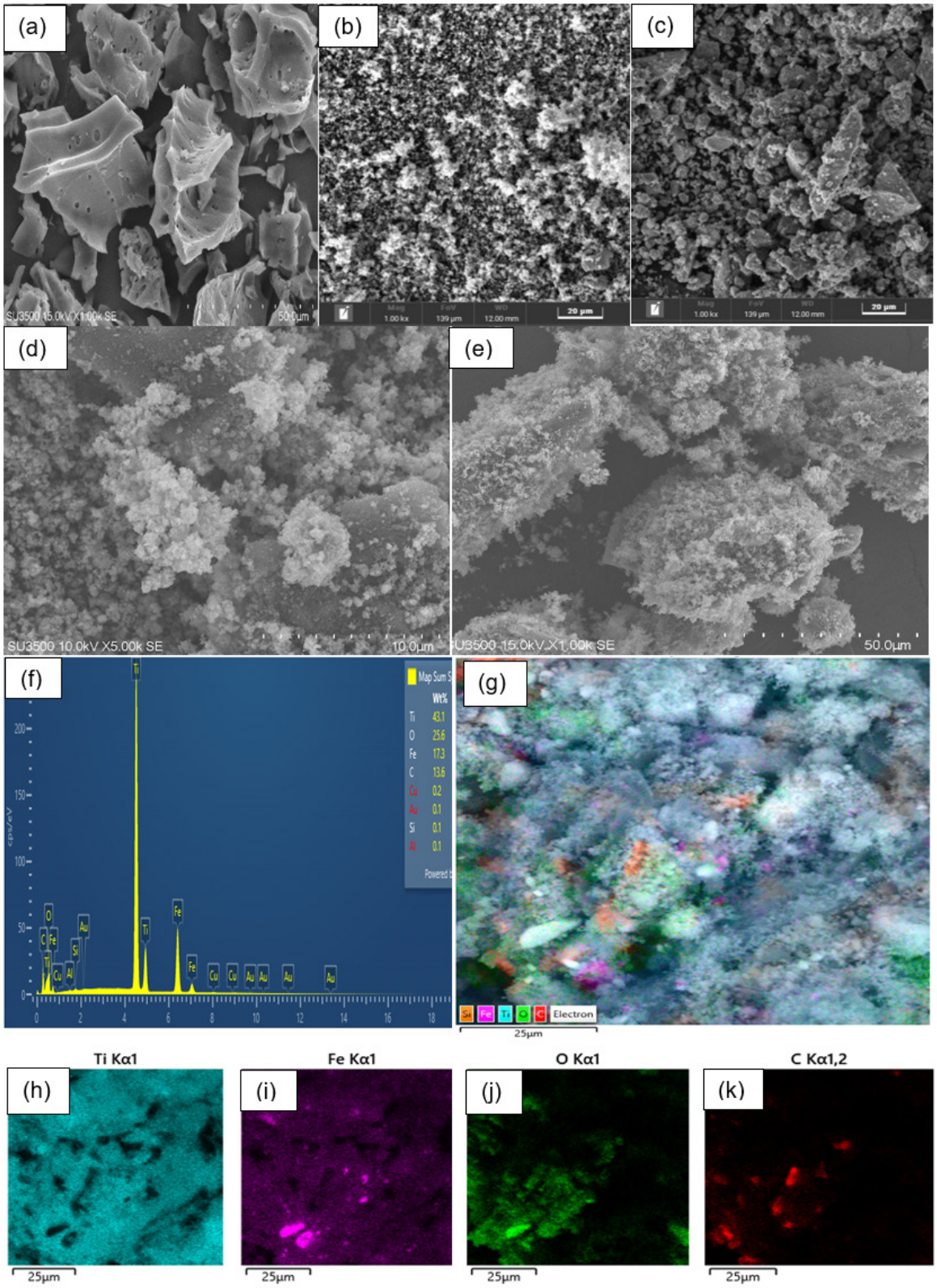


Fig. 9. SEM images of **(a)** Activated carbon, **(b)** TiO_2, **(c)** Fe_3O_4, **(e)** TiO_2/Fe_3O_4, **(e)** TiO_2/Fe_3O_4/AC and the EDX-mapping results (f-k) TiO_2/Fe_3O_4/AC

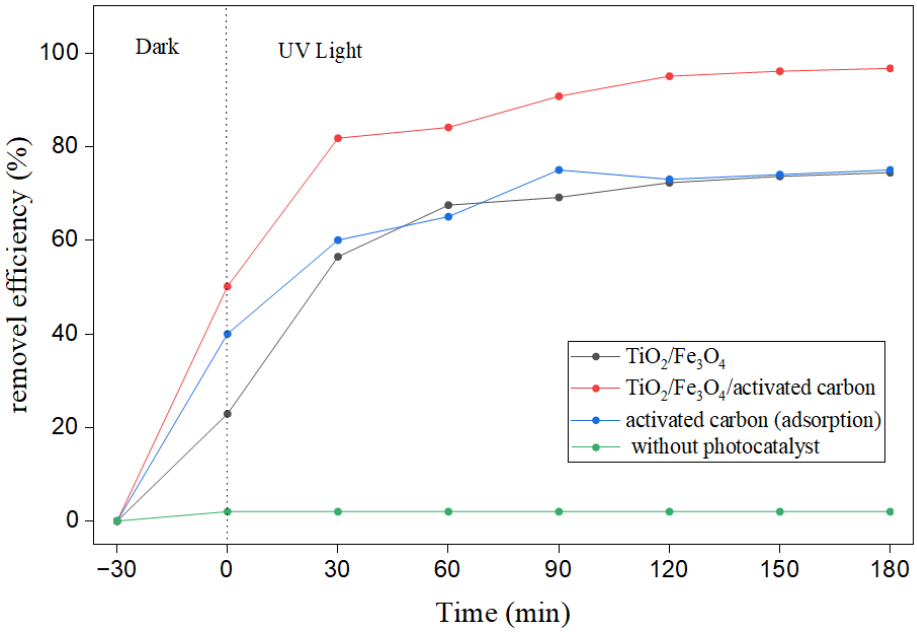


Fig. 10. Degradation efficiency of CR by TiO_2/Fe_3O_4 and TiO_2/Fe_3O_4/AC photocatalysts

Table 1. Rate constants **(k)** and correlation coefficients (R^2) for CR degradation kinetics based on pseudo-first-order and pseudo-second-order models.

sample	k_{a1}(L/mg)	R^2	k_{a2} (L/mg)	R^2
TiO_2/Fe_3O_4/ AC	0,0159	0.9528	0.2267	0.9408
TiO_2/Fe_3O_4	0.0065	0.8403	0.0246	0.9172

showed no significant decrease in concentration, indicating that pure photolysis was ineffective. After the photocatalytic degradation process, the total CR removal reached 74% for TiO_2/Fe_3O_4 and 96.7% for TiO_2/Fe_3O_4/AC. The enhanced photocatalytic efficiency of the TiO_2/Fe_3O_4/AC composite is attributed to the incorporation of AC, which can adsorb a greater number of CR molecules onto the photocatalyst surface. This process increases the probability of contact between dye molecules and the active sites of TiO_2, allowing the photocatalytic reaction to proceed more effectively under UV irradiation. Therefore, the improvement in CR degradation efficiency is not solely due to the photocatalytic activity of TiO_2/Fe_3O_4 but also to the adsorption capacity of AC, which synergistically enhances the overall performance of the composite [44]. The kinetics of CR degradation were analyzed during dark adsorption (−30 to 0 min) followed by photocatalysis (0–180 min). The rate constants were determined using the Langmuir–Hinshelwood (LH) pseudo-first-order and pseudo-second-order models (Equations 3 and 5) [44], with results presented in **Table 2**. The TiO_2/Fe_3O_4/AC composite exhibited higher degradation rates than TiO_2/Fe_3O_4, with the pseudo-first-order rate constant k_{a1} = 0.0159 min^{-1} (R^2 = 0.953) and the pseudo-second-order rate constant k_{a2} = 0.2267 L mg^{-1} min^{-1} (R^2 = 0.941). In comparison, TiO_2/Fe_3O_4 gave k_{a1} = 0.0065 min^{-1} (R^2 = 0.840) and k_{a2} = 0.0246 L mg^{-1} min^{-1} (R^2 = 0.917). These findings indicate that the pseudo-second-order model better fitted the kinetics of CR degradation by TiO_2/Fe_3O_4/AC.

$$ln\frac{C_0}{C_t} = k_{a1}t \quad (3)$$

$$\frac{1}{C_t} = \frac{1}{C_t} + k_{a2}t \quad (4)$$

where

Ct : the remaining concentration of CR dye at irradiation time t,
C0 : the initial concentration of CR dye after adsorption–desorption equilibrium,
k1 and k2: the apparent Langmuir–Hinshelwood pseudo-first-order and pseudo-second-order rate constants, respectively, and
t : is the irradiation time.

J Water Environ Nanotechnol, 2026, 11(4): 504-521
10.22090/jwent.2026.2077459.2005

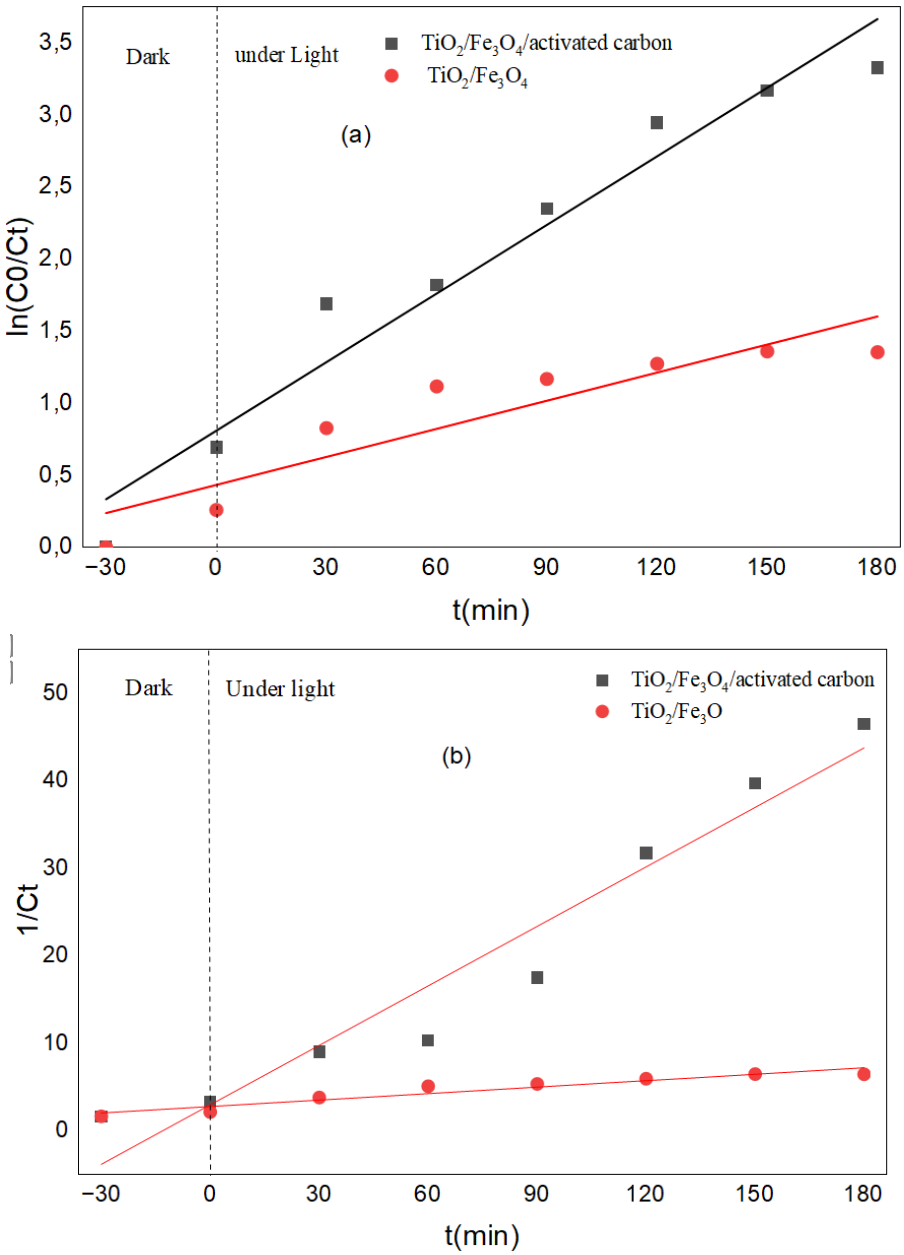


Fig. 11. Kinetics of CR degradation by TiO_2/Fe_3O_4 and TiO_2/Fe_3O_4/AC composites fitted to pseudo-first-order **(a)** and pseudo-second-order models **(b)**.

To further evaluate the photocatalytic performance of the synthesized TiO_2/Fe_3O_4/AC composite, a comparison with previous studies is presented in **Table 2**.

3.9 The efficiency of CR photocatalytic degradation is influenced by pH parameters

The initial pH of the solution is a critical parameter in the photocatalytic degradation process, as it strongly influences the degradation of CR. Variations in pH can alter the catalyst's surface charge and ionization state, thereby affecting interactions between the catalyst and dye molecules. Moreover, pH influences the dissociation of compounds and the distribution of charges on the catalyst surface, ultimately affecting photocatalytic performance [51]. The degradation performance of TiO_2/Fe_3O_4 and TiO_2/Fe_3O_4/AC composites was evaluated at different pH values ranging from 5 to 8 to compare their effectiveness in degrading CR. As shown in **Fig. 12**, photocatalytic efficiency decreased with increasing pH from 5 to 8. At lower pH, the catalyst surface becomes

Table 2. Comparison of TiO_2/Fe_3O_4/AC Photocatalysts with Previous Studies

Photocatalyst	Synthesis Method	Target Pollutant	Concentration	Light Source	Degradation Efficiency (%)	Reference
$Fe_3O_4/SiO_2/TiO_2$	-	Congo Red	10 mg/L	UV	96.52%	[45]
Fe_3O_4/rGO/TiO_2	Coprecipitation and modified Hummers with green synthesis route	Methylene blue	7 mg/L	UV	99.2 %	[46]
Fe-doped TiO_2	Sol-gel	Rhodamine B	5 mg/L	Visible	99,20%	[47]
TiO_2/ZnO-chitosan	A simple ex-situ mechanical mixing method	Methylene blue	10 mg/L	Visible	99%	[48]
TiO_2/AC	sol-gel	Paracetamol	10 mg/L	UV	95%	[49]
Fe_3O_4/TiO_2	coprecipitation	Methylene blue	10 mg/L	UV	99,9%	[50]
TiO_2/Fe_3O_4/AC	Simple physical mixing	Congo red	20 mg/L	UV	96.7%	This study

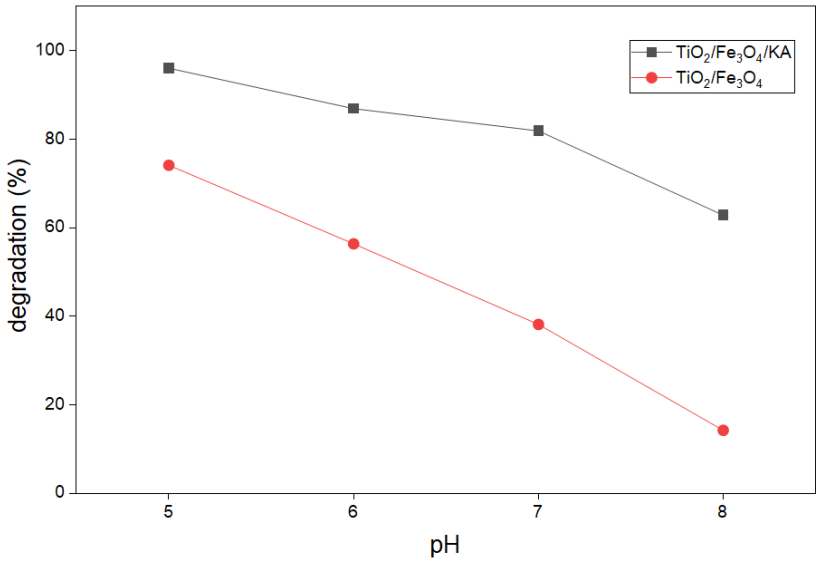


Fig. 12. Effect of pH on the photocatalytic degradation of CR using Fe_3O_4/TiO_2 and Fe_3O_4/TiO_2/AC catalysts.

positively charged due to the dominance of H^+ ions, resulting in electrostatic attraction with the anionic CR molecules and thereby accelerating photocatalytic degradation. In contrast, under alkaline conditions, the catalyst surface becomes negatively charged owing to the dominance of OH^- ions, leading to electrostatic repulsion that hinders adsorption and reduces photocatalytic activity [52]. At pH 5, the TiO_2/Fe_3O_4/AC composite achieved a degradation efficiency of 95.69%, whereas TiO_2/Fe_3O_4 reached approximately 74.7%.

3.10 Reusability of photocatalyst

The reusability of photocatalysts is a crucial aspect of the photodegradation process. Magnetic materials play a pivotal role, as they enable the composites to be rapidly separated from solutions using an external magnetic field, making the reuse of the composites more efficient. This study examines the recycling potential of the TiO_2/Fe_3O_4/AC composite for degrading CR dye solution. The findings are illustrated in **Fig. 13**, highlighting the composite's effectiveness over multiple cycles. After four cycles, the photodegradation efficiency of TiO_2/Fe_3O_4/AC decreased from 96.7% to 72%, representing a reduction of approximately 25%. This decline can be attributed to several factors, including material loss during recovery processes (e.g., washing), which may reduce the amount of photocatalyst available for subsequent cycles and diminish surface activity [31]. Furthermore, the properties of magnetic nanoparticles may change after several cycles due to particle aggregation, reducing the effective surface area and the

J Water Environ Nanotechnol, 2026, 11(4): 504-521
10.22090/jwent.2026.2077459.2005

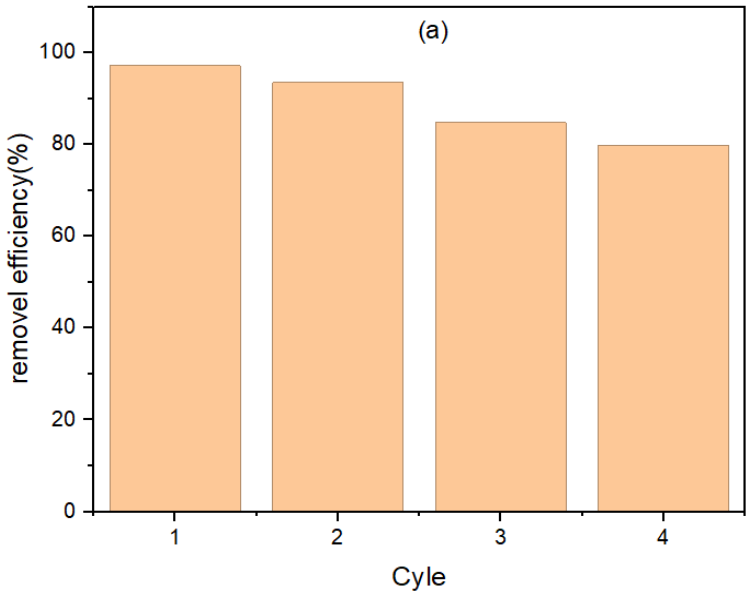


Fig. 13. Regeneration of TiO_2/Fe_3O_4/AC photocatalyst over multiple cycles

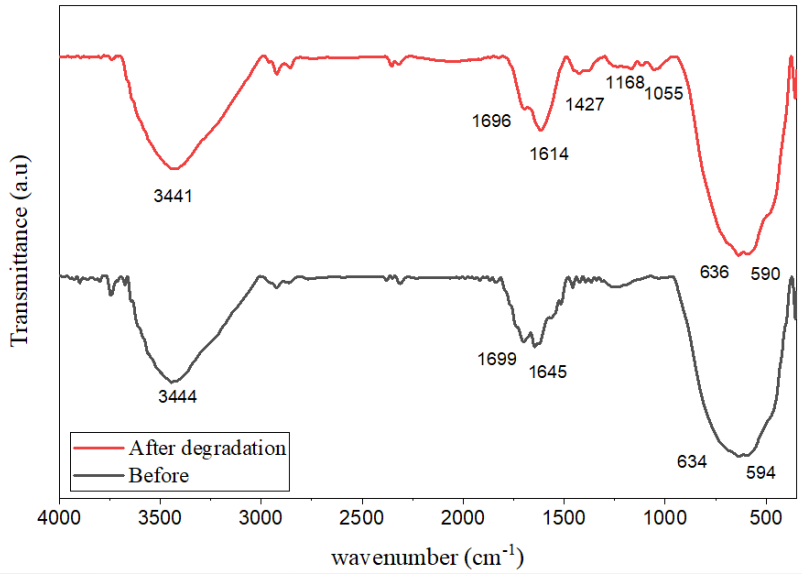


Fig. 14. FTIR characterization results of the TiO_2/Fe_3O_4/AC composite before and after 4 degradation cycles

number of active sites. Additionally, pore blockage and surface contamination can contribute to the decreased adsorption and photodegradation activity observed after repeated use [46].

The FTIR spectrum of the TiO_2/Fe_3O_4/AC composite after four cycles of degradation (**Fig. 14**) shows no significant changes in the absorption bands compared to the spectrum before use. The major absorption bands observed at 3441, 1695, 1614, 636, and 590 cm^{-1} remain essentially unchanged, indicating that the structural integrity of the composite is maintained throughout the repeated degradation cycles. However, sharp bands appear in the 1500–1000 cm^{-1} region, which indicates the presence of residual functional groups from CR molecules that remain adsorbed on the photocatalyst surface. This residual adsorption results in a slight reduction in the composite's overall adsorption and photocatalytic degradation performance.

3.10 Reaction Mechanism

The scavenger test results showed that the addition of IPA and $AgNO_3$ did not significantly affect the degradation efficiency, indicating that hydroxyl radicals (•OH) and electrons

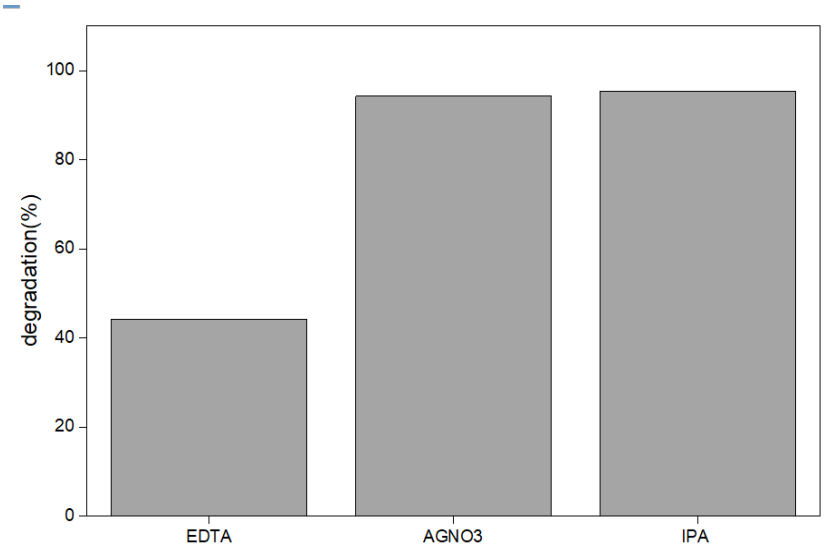


Fig. 15. Photodegradation of CR dye by TiO_2/Fe_3O_4/AC in the presence of a series of scavengers

(e^-) had minimal contribution to the photodegradation process of CR. In contrast, holes (h^+) acted as the primary oxidative species in the degradation of CR dye using a TiO_2/Fe_3O_4/AC photocatalyst (**Fig. 15**). These findings are consistent with the results reported by Delafrouz et al. (2024) [53]. This radical scavenging test provided fundamental information regarding the reactive species involved in the photocatalytic mechanism, thereby enhancing the understanding of the processes underlying the effectiveness of organic pollutant degradation.

The proposed reaction mechanism is as follows [54]:

$$\text{Photocatalyst} + hy \rightarrow e^-_{CB} + h^+_{VB} \quad (5)$$

$$O + e^-_{CB} \rightarrow \bullet O_2^- \quad (6)$$

$$\bullet O_2^- \rightarrow H_2O \rightarrow HO_2^{\bullet} + OH^- \quad (7)$$

$$OH^- + h^+_{VB} \rightarrow \bullet OH \quad (8)$$

$$\bullet O_2^- + h^+_{VB} + CR \rightarrow \text{degradation products } (CO_2 + H_2O) \quad (9)$$

The process begins with the adsorption of CR molecules onto the photocatalyst surface, establishing an equilibrium between CR and the active sites. When TiO_2 is irradiated with UV light, electrons (e^-) in the valence band (VB) are excited to the conduction band (CB), leaving holes (h^+) in the VB. AC enhances this process by adsorbing more CR molecules in proximity to TiO_2, increasing their contact with active sites and creating a synergistic effect between adsorption and photodegradation [55], [56]. Fe_3O_4 not only serves as a magnetic component for facile catalyst recovery but also facilitates electron transfer from TiO_2 to AC, thereby reducing electron–hole recombination [24], [46], [57]. In addition, AC acts as an electron sink, transferring the photoexcited electrons to dissolved oxygen to form reactive oxygen species ($\bullet O_2^-$), while the holes (h^+) react with hydroxide ions (OH^-) or adsorbed water molecules to produce hydroxyl radicals ($\bullet OH$). Both species contribute significantly to the oxidative degradation of CR [58].

4. CONCLUSIONS

The TiO_2/Fe_3O_4/AC composite was successfully synthesized using a simple physical mixing method. The synergy between Fe_3O_4, AC, and TiO_2 produces a material that is effective, stable, and reusable for the efficient photodegradation of CR dye. The composite exhibited a degradation efficiency of 96.7%, which is significantly higher than that of TiO_2/Fe_3O_4, which achieved 74%. This improvement is attributed to the high adsorption capacity of AC and the magnetic separation capability provided by Fe_3O_4. The incorporation of AC into TiO_2 also contributes to the enhancement of photodegradation activity by increasing the surface area and facilitating faster electron transfer during the reaction. Moreover, the magnetic properties of Fe_3O_4 enable efficient separation of the material using an external magnetic field, supporting reusability and sustainability in the photodegradation process. After four regeneration cycles, the degradation efficiency decreased from 96.7% to 72%; nevertheless, the composite still demonstrated good structural and functional stability upon repeated use. Based on these findings, the TiO_2/Fe_3O_4/AC composite shows excellent potential as a photocatalyst for degrading various anionic and cationic organic pollutants.

Conflict of Interest
The authors declare that they have no known competing financial interests

J Water Environ Nanotechnol, 2026, 11(4): 504-521
10.22090/jwent.2026.2077459.2005

or personal relationships that could have appeared to influence the work reported in this paper.

Acknowledgements

The author would like to express their appreciation to Kementerian Pendidikan, Kebudayaan, Riset dan Teknologi DIKTI Indonesia for their financial backing through the Thesis Research Magister program (Contract Number: 02209/UN4.22/PT.01.03/2025). Gratitude is also extended to Microsoft Copilot for its help with language editing, grammar enhancements, and clarifying the manuscript. The authors have thoroughly reviewed and approved all content supported by AI to maintain scientific precision and honesty.

REFERENCES

[1] R. Rajendran, O. Rojviroon, P. Arumugam, G. Ramasamy, S. Paramasivam, and T. Rojviroon, "Synergistic effects of activated Carbon-Supported TiO_2/ZnO nanocomposites for photocatalytic dye degradation and antibacterial activity," *J Mol Liq*, vol. 433, pp. 1–11, Sep. 2025, https://doi.org/10.1016/j.molliq.2025.127792.

[2] A. S. M. Nur *et al.*, "A review on the development of elemental and codoped TiO_2 photocatalysts for enhanced dye degradation under UV–vis irradiation," *Journal of Water Process Engineering*, Jun. 01, 2022, *Elsevier Ltd*. https://doi.org/10.1016/j.jwpe.2022.102728.

[3] F. Riyanti, H. Hasanudin, A. Rachmat, W. Purwaningrum, and P. L. Hariani, "Photocatalytic degradation of methylene blue and Congo red dyes from aqueous solutions by bentonite-Fe3O4 magnetic," *Communications in Science and Technology*, vol. 8, no. 1, pp. 1–9, 2023, https://doi.org/10.21924/cst.8.1.2023.1007.

[4] S. N. N. M. Makhtar, N. Yusof, N. Fajrina, N. H. H. Hairom, F. Aziz, and W. N. Wan Salleh, "V_2O_5/Cds as nanocomposite catalyst for Congo red dye photocatalytic degradation under visible light," in *Materials Today: Proceedings*, Elsevier Ltd, 2024, pp. 1–4. https://doi.org/10.1016/j.matpr.2023.10.152.

[5] N. Asses, L. Ayed, N. Hkiri, and M. Hamdi, "Congo Red Decolorization and Detoxification by Aspergillus Niger: Removal Mechanisms and Dye Degradation Pathway," *Biomed Res Int*, vol. 2018, pp. 1–9, 2018, https://doi.org/10.1155/2018/3049686.

[6] S. Charafi, F. Z. Janani, A. Elhalil, M. Abdennouri, M. Sadiq, and N. Barka, "Optimization of photocatalytic degradation of amoxicillin by ZnO-TiO_2 heterojunction under UV-Visible irradiation," *Cleaner Chemical Engineering*, vol. 11, pp. 1–14, Dec. 2025, https://doi.org/10.1016/j.clce.2025.100183.

[7] A. Saefumillah, B. S. Mahadika, Saepurahman, K. A. Kurnia, D. V. Wellia, and D. O. B. Apriandanu, "Adsorption and photodegradation of various organic dyes in batch and flow systems over TiO_2-chitosan immobilized on glass beads," *Results in Surfaces and Interfaces*, vol. 18, pp. 1–11, Jan. 2025, https://doi.org/10.1016/j.rsurfi.2025.100418.

[8] P. D. Sanadi *et al.*, "Controllable synthesis of semiconducting anatase TiO_2 nanostructures for visible light driven photocatalytic degradation of crystal violet and methylene blue dye," *Spectrochim Acta A Mol Biomol Spectrosc*, vol. 341, pp. 1–11, Nov. 2025, https://doi.org/10.1016/j.saa.2025.126404.

[9] W. Chen, L. Chang, S. Bin Ren, Z. C. He, G. B. Huang, and X. H. Liu, "Direct Z-scheme 1D/2D WO2.72/$ZnIn_2S_4$ hybrid photocatalysts with highly-efficient visible-light-driven photodegradation towards tetracycline hydrochloride removal," *J Hazard Mater*, vol. 384, pp. 1–11, Feb. 2020, https://doi.org/10.1016/j.jhazmat.2019.121308.

[10] N. Kousar *et al.*, "Efficient synergistic degradation of Congo red and omeprazole in wastewater using rGO/Ag@ZnO nanocomposite," *Journal of Water Process Engineering*, vol. 58, pp. 1–14, Feb. 2024, https://doi.org/10.1016/j.jwpe.2024.104775.

[11] M. Utami, H. A. Zahra', Khoirunisa, and T. A. Dewi, "Green synthesis of magnetic activated carbon from peanut shells functionalized with TiO_2 photocatalyst for Batik liquid waste treatment," *Open Chem*, vol. 20, no. 1, pp. 1229–1238, Jan. 2022, https://doi.org/10.1515/chem-2022-0231.

[12] J. You, C. Liu, X. Feng, B. Lu, L. Xia, and X. Zhuang, "In situ synthesis of ZnS nanoparticles onto cellulose/chitosan sponge for adsorption–photocatalytic removal of Congo red," *Carbohydr Polym*, vol. 288, pp. 1–19, Jul. 2022, https://doi.org/10.1016/j.carbpol.2022.119332.

[13] Y. Li *et al.*, "Powering efficient dye degradation based on nanostructured FeOOH/TiO_2 composite with hydrophilic surfaces and unparalleled photocatalytic performance," *Ceram Int*, vol. 51, no. 11, pp. 14966–14973, May 2025, https://doi.org/10.1016/j.ceramint.2025.01.340.

[14] S. Y. Lee and S. J. Park, "TiO_2 photocatalyst for water treatment applications," Nov. 25, 2013. https://doi.org/10.1016/j.jiec.2013.07.012.

[15] Q. Guo, C. Zhou, Z. Ma, and X. Yang, "Fundamentals of TiO_2 Photocatalysis: Concepts, Mechanisms, and Challenges," Dec. 01, 2019, *Wiley-VCH Verlag*. https://doi.org/10.1002/adma.201901997.

[16] S. N. Sadikin *et al.*, "Photocatalytic activity and stability properties of porous TiO_2 film as photocatalyst for methylene blue and methylene orange degradation," *Int J Electrochem Sci*, vol. 18, no. 9, pp. 1–8, 2023, https://doi.org/10.1016/j.ijoes.2023.100246.

[17] R. Rashid *et al.*, "Advancements in TiO_2-based photocatalysis for environmental remediation: Strategies for enhancing visible-light-driven activity," 2024, *Elsevier Ltd*. https://doi.org/10.1016/j.chemosphere.2023.140703.

[18] S. Ali *et al.*, "Synthesis of activated carbon-supported TiO_2-based nano-photocatalysts with well recycling for efficiently degrading high-concentration pollutants," *Catal Today*, vol. 335, pp. 557–564, Sep. 2019, https://doi.org/10.1016/j.cattod.2019.03.044.

[19] A. Spoială *et al.*, "Preparation and Characterization of Chitosan/TiO_2 Composite Membranes as Adsorbent Materials for Water Purification," *Membranes (Basel)*, vol. 12, no. 8, pp. 1–25, Aug. 2022, https://doi.org/10.3390/membranes12080804.

[20] X. Liu, Y. Liu, S. Lu, W. Guo, and B. Xi, "Performance and mechanism into TiO_2/Zeolite composites for sulfadiazine adsorption and photodegradation," *Chemical Engineering Journal*, vol. 350, pp. 131–147, Oct. 2018, https://doi.org/10.1016/j.cej.2018.05.141.

[21] B. D. Napruszewska, D. Duraczyńska, J. Kryściak-Czerwenka, P. Nowak, and E. M. Serwicka, "Clay Minerals/TiO_2 Composites—Characterization and Application in Photocatalytic Degradation of Water Pollutants," *Molecules*, vol. 29, no. 20, pp. 1–20, Oct. 2024, https://doi.org/10.3390/molecules29204852.

[22] M. Baruah, S. Kumar, S. L. Ezung, L. Jamir, U. Bora Sinha, and D. Sinha, "Preparation of Co-doped TiO_2 activated carbon nanocomposite and its photocatalytic degradation of phenol wastewater," *Inorg Chem Commun*, vol. 166, pp. 1–13, Aug. 2024, https://doi.org/10.1016/j.inoche.2024.112644.

[23] E. Aghababaei, M. Alizadeh, and A. Bahrami, "Synthesis and characterization of Ce-doped TiO_2/Cu-doped Fe_3O_4 heterogeneous

photocatalyst for antibacterial applications and visible-light photocatalytic degradation of methylene blue," *Ceram Int*, pp. 1–19, 2025, https://doi.org/10.1016/j.ceramint.2025.05.109.

[24] V. T. T. Thuy *et al.*, "Degradation of enrofloxacin in water by Fe_3O_4@TiO_2 magnetic photocatalyst: optimization of environmental factors," *Desalination Water Treat*, vol. 287, pp. 124–138, Mar. 2023, https://doi.org/10.5004/dwt.2023.29351.

[25] E. Savitri, S. W. Yunita, C. Winoto, and R. K. Widi, "Innovative Waste Benzene Remediation by Enhanced Photocatalytic with TiO_2/Fe_3O_4-Based Material Supported by Bentonite in Batch and Continuous System," *Trends in Sciences*, vol. 21, no. 7, pp. 1–13, Jul. 2024, https://doi.org/10.48048/tis.2024.7872.

[26] D. Ramutshatsha-Makhwedzha, M. L. Mavhungu, J. Baloyi, and R. Mbaya, "Synthesis and characterization of Fe_3O_4@TiO_2@ Zeolite nanocomposite adsorbent for the removal of Levoflaxin antibiotic from environmental water matrices," *Journal of the Iranian Chemical Society*, vol. 22, no. 1, pp. 113–128, Jan. 2025, https://doi.org/10.1007/s13738-024-03135-2.

[27] A. V. Tajareh, H. Ganjidoust, and B. Ayati, "Synthesis of TiO_2/Fe_3O_4/MWCNT Magnetic and Reusable Nanocomposite with High Photocatalytic Performance in the Removal of Colored Combinations from Water," *Journal of Water and Environmental Nanotechnology*, vol. 4, no. 3, pp. 198–212, Jun. 2019, https://doi.org/10.22090/jwent.2019.03.003.

[28] M. A. Lala, Z. O. Olomowewe, A. T. Adeniyi, and A. Giwa, "Maize cob-derived activated carbon as an adsorbent for the removal of nickel (II) cation from aqueous solution: optimization and kinetic studies," *Arab J Basic Appl Sci*, vol. 30, no. 1, pp. 573–582, Dec. 2023, https://doi.org/10.1080/25765299.2023.2266230.

[29] N. Ahmad, F. Suryani Arsyad, I. Royani, and A. Lesbani, "Adsorption of methylene blue on magnetite humic acid: Kinetic, isotherm, thermodynamic, and regeneration studies," *Results Chem*, vol. 4, pp. 1–0, Jan. 2022, https://doi.org/10.1016/j.rechem.2022.100629.

[30] Ramalingam s, "Synthesis of Nanosized Titanium Dioxide (TiO_2) by Sol-Gel Method," *International Journal of Innovative Technology and Exploring Engineering*, vol. 9, pp. 732–735, Dec. 2019, https://doi.org/10.35940/ijitee.b1174.1292s219.

[31] S. Moosavi *et al.*, "Methylene blue dye photocatalytic degradation over synthesised fe3 o4 /ac/tio2 nano-catalyst: Degradation and reusability studies," *Nanomaterials*, vol. 10, no. 12, pp. 1–15, Dec. 2020, https://doi.org/10.3390/nano10122360.

[32] Y. L. Pang, S. Lim, and R. K. L. Lee, "Enhancement of sonocatalytic degradation of organic dye by using titanium dioxide (TiO_2)/activated carbon (AC) derived from oil palm empty fruit bunch," *Environmental Science and Pollution Research*, vol. 27, no. 28, pp. 1–15, Oct. 2019, https://doi.org/10.1007/s11356-019-05373-x.

[33] S. T. Almutairi, "Fabrication and catalytic activity of TiO_2/Fe_3O_4 and Fe_3O_4/β-cyclodextrin nanocatalysts for safe treatment of industrial wastewater," *Heliyon*, vol. 10, no. 15, pp. 1–12, Aug. 2024, https://doi.org/10.1016/j.heliyon.2024.e35400.

[34] H. Pishrafti, H. Kamani, N. Mansouri, A. H. Hassani, and H. Ahmadpanahi, "Photocatalytic removal of the erythromycin antibiotic using Fe-doped TiO2 @Fe3 O4 magnetic nanoparticles: investigation of effective parameters, process kinetics and degradation end products," *Desalination Water Treat*, vol. 262, pp. 323–337, Jun. 2022, https://doi.org/10.5004/dwt.2022.28542.

[35] W. Alamaw, A. M. Taddesse, A. Adgo, Z. Bezu, and E. Teju, "Synthesis and characterization of zeolite-supported CdS/TiO2/Ag2CO3 ternary composite for Photodegradation of methyl Orange," *Results Chem*, vol. 14, pp. 1–15, Mar. 2025, https://doi.org/10.1016/j.rechem.2025.102063.

[36] P. Ozpinar *et al.*, "Effect of binder on the electrochemical performance of activated carbon electrodes obtained from waste hazelnut shells: Comparison of PTFE and PVDF," *Diam Relat Mater*, vol. 137, pp. 1–34, Aug. 2023, https://doi.org/10.1016/j.diamond.2023.110092.

[37] S. Kumar, S. Baruah, and A. Puzari, "Poly(p-phenylenediamine)-based nanocomposites with metal oxide nanoparticle for optoelectronic and magneto-optic application," *Polymer Bulletin*, vol. 77, no. 1, pp. 441–457, Jan. 2020, https://doi.org/10.1007/s00289-019-02760-9.

[38] E. A. Al-Oubidy and F. J. Kadhim, "Photocatalytic activity of anatase titanium dioxide nanostructures prepared by reactive magnetron sputtering technique," *Opt Quantum Electron*, vol. 51, no. 1, pp. 1–23, Jan. 2019, https://doi.org/10.1007/s11082-018-1738-z.

[39] L. de O. Pereira, I. M. Sales, L. P. Zampiere, S. S. Vieira, I. do R. Guimarães, and F. Magalhães, "Preparation of magnetic photocatalysts from TiO2, activated carbon and iron nitrate for environmental remediation," *J Photochem Photobiol A Chem*, vol. 382, pp. 1–9, Sep. 2019, https://doi.org/10.1016/j.jphotochem.2019.111907.

[40] G. Byzynski, D. P. Volanti, C. Ribeiro, V. R. Mastelaro, and E. Longo, "Direct photo-oxidation and superoxide radical as major responsible for dye photodegradation mechanism promoted by TiO2–rGO heterostructure," *Journal of Materials Science: Materials in Electronics*, vol. 29, no. 19, pp. 17022–17037, Oct. 2018, https://doi.org/10.1007/s10854-018-9799-0.

[41] B. Toubal, R. Bensaha, and F. Yakuphanoglu, "The influence of copper-cobalt co-doping on optical and electrical properties of nanostructures TiO2 thin films prepared by sol-gel," *J Solgel Sci Technol*, vol. 82, no. 2, pp. 478–489, May 2017, https://doi.org/10.1007/s10971-017-4337-8.

[42] A. A. Ali, I. S. Ahmed, and E. M. Elfiky, "Auto-combustion Synthesis and Characterization of Iron Oxide Nanoparticles (α-Fe2O3) for Removal of Lead Ions from Aqueous Solution," *J Inorg Organomet Polym Mater*, vol. 31, no. 1, pp. 384–396, Jan. 2021, https://doi.org/10.1007/s10904-020-01695-3.

[43] S. Bassim, A. K. Mageed, A. A. AbdulRazak, and H. Sh. Majdi, "Green Synthesis of Fe3O4 Nanoparticles and Its Applications in Wastewater Treatment," *Inorganics (Basel)*, vol. 10, no. 12, pp. 1–23, Dec. 2022, https://doi.org/10.3390/inorganics10120260.

[44] S. N. U. S. Bukhari *et al.*, "Activated carbon based TiO2 nanocomposites (TiO2@AC) used simultaneous adsorption and photocatalytic oxidation for the efficient removal of Rhodamine-B (Rh–B)," *Ceram Int*, vol. 50, no. 21, pp. 41285–41298, 2024, https://doi.org/10.1016/j.ceramint.2024.07.440.

[45] P. L. Hariani, S. Salni, M. Said, and R. Farahdiba, "Core-shell Fe3O4/SiO2/TiO2 Magnetic Modified Ag for the Photocatalytic Degradation of Congo Red Dye and Antibacterial Activity," *Bulletin of Chemical Reaction Engineering & Catalysis*, vol. 18, no. 2, pp. 315–330, Aug. 2023, https://doi.org/10.9767/bcrec.19275.

[46] H. P. Kusumah *et al.*, "Eco-friendly TiO2-doped Fe3O4/rGO nanocomposites synthesized using plant extracts for

photodegradation of organic dye," *Carbon Resources Conversion*, pp. 1–15, Sep. 2025, https://doi.org/10.1016/j.crcon.2025.100373.

[47] E. T. Wahyuni, S. Annur, N. D. Lestari, and M. Mudasir, "Conversion of iron rusty waste into Fe dopant of TiO2 to increase its photocatalytic activity under visible light for photodegradation of rhodamine-B," *Results in Engineering*, vol. 22, pp. 1–9, Jun. 2024, https://doi.org/10.1016/j.rineng.2024.102296.

[48] M. A. Mohd Adnan, M. F. Majnis, M. A. Mat Norman, M. D. A. Rahman, M. R. Johan, and N. Muhd Julkapli, "Visible-light-activated TiO2/ZnO-chitosan catalyst for photodegradation of methylene blue dye: An experimental and predictive modelling using artificial neural networks," *Journal of Water Process Engineering*, vol. 77, pp. 1–18, Sep. 2025, https://doi.org/10.1016/j.jwpe.2025.108423.

[49] D. C. S. Gloria *et al.*, "Preparation of TiO2/activated carbon nanomaterials with enhanced photocatalytic activity in paracetamol degradation," *Mater Chem Phys*, vol. 305, pp. 1–8, Sep. 2023, https://doi.org/10.1016/j.matchemphys.2023.127947.

[50] R. M. Tumbelaka, N. I. Istiqomah, T. Kato, D. Oshima, and E. Suharyadi, "High reusability of green-synthesized Fe3O4/TiO2 photocatalyst nanoparticles for efficient degradation of methylene blue dye," *Mater Today Commun*, vol. 33, pp. 1–15, Dec. 2022, https://doi.org/10.1016/j.mtcomm.2022.104450.

[51] M. F. Hanafi and N. Sapawe, "Effect of pH on the photocatalytic degradation of remazol brilliant blue dye using zirconia catalyst," *Mater Today Proc*, vol. 31, pp. 260–262, 2020, https://doi.org/10.1016/j.matpr.2020.05.746.

[52] N. Khera and P. Jeevanandam, "Core-shell composite nanoarchitectonics of TiO2@NiCo2S4 via thermal decomposition approach for photodegradation of congo red," *Environ Res*, vol. 274, pp. 1–13, Jun. 2025, https://doi.org/10.1016/j.envres.2025.121304.

[53] S. Delafrouz, M. Hasheminiasari, S. Alamolhoda, and S. M. Masoudpanah, "Role of fuel's mixture on photocatalytic performance of g-C3N4/TiO2 nanocomposites," *Heliyon*, vol. 10, no. 22, Nov. 2024, https://doi.org/10.1016/j.heliyon.2024.e40464.

[54] Z. Li *et al.*, "Preparation of heterogeneous TiO2/g-C3N4 with a layered mosaic stack structure by use of montmorillonite as a hard template approach: TC degradation, kinetic, mechanism, pathway and DFT investigation," *Appl Clay Sci*, vol. 207, p. 106107, Jun. 2021, https://doi.org/10.1016/j.clay.2021.106107.

[55] Y. Yue *et al.*, "Synergistic adsorption and photocatalysis study of TiO2 and activated carbon composite," *Heliyon*, vol. 10, no. 10, pp. 1–13, May 2024, https://doi.org/10.1016/j.heliyon.2024.e30817.

[56] L. Wenbin, Z. Zhou, Z. Chen, L. Chen, J. Tang, and L. Zhang, "Adsorption and degradation of tetracycline hydrochloride in aqueous solutions using activated carbon with Fe/Ag nanoparticles," *Mater Today Commun*, vol. 39, pp. 1–15, Jun. 2024, https://doi.org/10.1016/j.mtcomm.2024.108504.

[57] S. N. Yahya *et al.*, "Photodegradation of organic water pollutants using magnetically separable and reusable novel Ag-doped Fe3O4/TiO2 nanocomposites synthesized by green route," *Inorg Chem Commun*, vol. 172, pp. 1–15, Feb. 2025, https://doi.org/10.1016/j.inoche.2024.113749.

[58] M. Moshari, M. Rabbani, and R. Rahimi, "Synthesis of TCPP–Fe3O4@S/RGO and its application for purification of water," *Research on Chemical Intermediates*, vol. 42, no. 6, pp. 5441–5455, Jun. 2016, https://doi.org/10.1007/s11164-015-2378-6.